Modeling the dielectric strength variation of supercritical fluids driven by cluster formation near critical point

Cite as: Phys. Fluids **32**, 077101 (2020); https://doi.org/10.1063/5.0008848
Submitted: 25 March 2020 . Accepted: 08 June 2020 . Published Online: 01 July 2020

Farhina Haque, Jia Wei (魏嘉), Lukas Graber, and Chanyeop Park

Physics of Fluids ARTICLE scitation.org/journal/phf

Modeling the dielectric strength variation of supercritical fluids driven by cluster formation near critical point

Cite as: Phys. Fluids 32, 077101 (2020); doi: 10.1063/5.0008848
Submitted: 25 March 2020 • Accepted: 8 June 2020 •
Published Online: 1 July 2020

Farhina Haque,[1] Jia Wei (魏嘉),[2] Lukas Graber,[2] and Chanyeop Park[1,a)]

AFFILIATIONS

[1] Department of Electrical and Computer Engineering, Mississippi State University, Mississippi State, Mississippi 39762-6334, USA
[2] School of Electrical and Computer Engineering, Georgia Institute of Technology, Atlanta, Georgia 30332, USA

[a)] **Author to whom correspondence should be addressed**: chanyeop.park@ece.msstate.edu

ABSTRACT

Density fluctuation driven by cluster formation causes drastic changes in the dielectric breakdown characteristics of supercritical fluids that cannot be described solely based on the conventional Townsend's gas discharge theory and Paschen's law. In this study, we model the dielectric breakdown characteristics of supercritical CO_2 as a function of pressure based on the electron scattering cross section data of CO_2 clusters that vary in size as a function of temperature and pressure around the critical point. The electron scattering cross section data of CO_2 clusters are derived from those of gaseous CO_2. We solve the Boltzmann equation based on the electron scattering cross section data to obtain critical electrical fields of various cluster sizes as a function of pressure. To validate our model, we compare the modeled breakdown voltage with the experimental breakdown measurements of supercritical CO_2, which show close agreement.

I. INTRODUCTION

Supercritical fluids (SCFs) that are achieved above the critical point have densities comparable to liquids.[1,2] Their high density results in high dielectric strength, which is essential for the materialization of high-voltage applications. In addition to high dielectric strength, the effective heat transfer properties of SCFs are ideal for high-power-density applications that require powerful cooling media that remove the heat generated by Joule heating. Owing to these advantages, researchers have been showing increasing interest in utilizing SCFs as insulating media in power applications.[3,4] The effects of electrode geometry and voltage polarity on the dielectric strength of SCFs have been reported in Refs. 5–10. Historically, SCFs are known as cluster fluids for their tendency to form clusters near the critical point.[11] The formation of clusters near the critical point results in substantial density fluctuation. Studies reported in the literature experimentally confirmed that density fluctuation caused by clustering effect leads to noticeable changes in the dielectric strength characteristics of SCFs.[11–15] The authors reported the correlation between breakdown voltage and density fluctuation in SCFs. Their dielectric strength modeling method is mainly based on the drastic changes in the isothermal compressibility of fluids near the critical point retrieved from the National Institute of Standards and Technology (NIST) database of thermophysical properties of fluid systems.[16] However, the reliance on the isothermal compressibility data makes dielectric strength modeling difficult for fluids whose isothermal compressibility data are unavailable in the database.

In this study, we develop a correlation between the breakdown characteristics of SCFs and the clustering effect. The electron scattering cross section data of SCFs modified from those of gas are derived based on the cluster size.[17] We use the electron scattering cross section data of gaseous CO_2[18] to derive those of supercritical CO_2 of various cluster sizes. Boltzmann analysis, a widely used method for describing electron kinetics,[19–22] is used to estimate the dielectric strength based on the electron scattering cross section data of supercritical CO_2 clusters of various sizes. The density-normalized ionization coefficients and density-normalized attachment coefficients are determined by solving the Boltzmann equation with the two term approximation.[23] We use the density-normalized critical electric fields of various supercritical clusters to represent the dielectric strength of supercritical CO_2. To validate our modeling approach, we compare the critical electric field values of our model with

experimental measurements reported in the literature.[12] The modeled results show close agreement with the experimental values by accurately estimating the drastic decline of dielectric strength near the critical point.

II. MODELING

To obtain the cross section data of clusters from those of gas, we assume that clusters are spheres with radius R_c, as shown in Fig. 1. Impact parameter h is a normal distance between the electron path and the center of a cluster, and A is where electron enters a cluster. Collision processes occurring between points B and B' on the electron trajectory are the basis of modeling the cross section data of clusters. The following equation derives the electron scattering cross section σ of a cluster with N number of molecules (i.e., cluster size):[17]

$$\sigma(N, W_{e0}) = \left[2\pi \int_0^{R_c} h\left\{1 - \exp\left[-n_0 \int_0^{2\sqrt{(R_c^2 - h^2)}} \sigma_0(1, W_e(x))F(x)dx\right]\right\}dh\right]/N, \quad (1)$$

where W_{e0} is the initial electron energy upon impact, $\sigma(N, W_{e0})$ is the electron scattering cross section data of cluster, R_c is the radius of the cluster, n_0 is the molecular density of the cluster, $\sigma_0(1, W_e(x))$ is the electron scattering cross section data of gas, and $F(x)$ is the probability of secondary electrons produced by ionization processes escaping out of the clusters. Note that $F(x)$ only applies to ionization collision processes. The electron scattering cross section data of a cluster are derived using those of a gas molecule at each position along the electron trajectory. Electron energy $W_e(x)$ at position x accounts for electron energy loss occurring inside clusters as the electron traverses along the electron trajectory. Electron energy loss in clusters is modeled as follows:

$$W_e = W_{e0} - \int_0^x \left(\frac{dW_e}{ds}\right)ds, \quad (2)$$

where W_{e0} is the electron energy at the moment of impact with a cluster and dW_e/ds is the energy loss rate of electron traversing in a cluster. For electron energies greater than 80 eV, we use Bethe's formula to model the electron energy loss rate, as shown in the following equation:

$$\frac{dW_e}{ds} \cong -\frac{\alpha_1 z}{W_e}\ln\left(\frac{\alpha_2 W_e}{z}\right) \text{ eV m} - 1, \quad (3)$$

where $\alpha_1 = k_1 q^2 n/(8\pi\varepsilon_0)$, W_e is the electron energy, n is the density of the cluster, k_1 is the empirical factor of correction, z is the atomic number, and q is the elementary charge. For CO_2, k_1 is 1.[17] On the other hand, for electron energy below 80 eV, Bethe's formula can no longer represent the electron energy loss rate due to its inaccuracy at energies below mean excitation energy.[24] Thus, for electron energies lower than 80 eV, all energy loss mechanisms including ionization, excitation, and momentum transfer processes are included in modeling the rate of electron energy loss,

$$\frac{dW_e}{ds} \cong -n\sigma_\tau\left((V_i + W_{s0})\alpha_i + \sum_{m,n} V^*_{m,n}a_{m,n} + 2\frac{m_e}{M}W_e\alpha_d\right), \quad (4)$$

where σ_τ is the total collision cross section, $\alpha_i\sigma_\tau$ is the ionization cross section, W_{s0} is the mean initial energy of an electron ejected by an ionization collision, $\alpha_{m,n}\sigma_\tau$ is the excitation cross section, $\alpha_d\sigma_\tau$ is the momentum transfer cross section, V_i is the ionization potential, $V_{m,n}$ is the excitation potential, m_e is the mass of an electron, and M is the mass of a neutral. Probability $F(x)$ can be modeled in three different ways: a linear model, a two-dimensional circular model, and a three-dimensional spherical model. Since clusters are spheres, we use the three-dimensional spherical model for $F(x)$. As shown in Fig. 2, we use spherical volumes evolving with radii $(x_{max} - x)/2$ with the traversing electron to represent the probability function as follows:

$$F(x) = (V_{cluster} - V_{sphere})/V_{cluster}, \quad (5)$$

where $V_{cluster}$ is the volume of the cluster and V_{sphere} is the of the sphere defined as

$$V_{sphere} = \frac{4}{3}\pi\left(\frac{x_{max} - x}{2}\right)^3, \quad (6)$$

where x is the distance traveled by the electron along the trajectory and x_{max} is the length of the electron trajectory with distance h from the cluster center defined as

$$x_{max} = 2\sqrt{(R_c^2 - h^2)}, \quad (7)$$

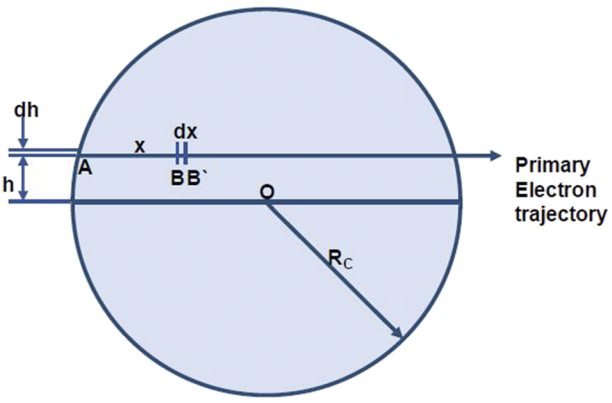

FIG. 1. Electron-cluster collision model.

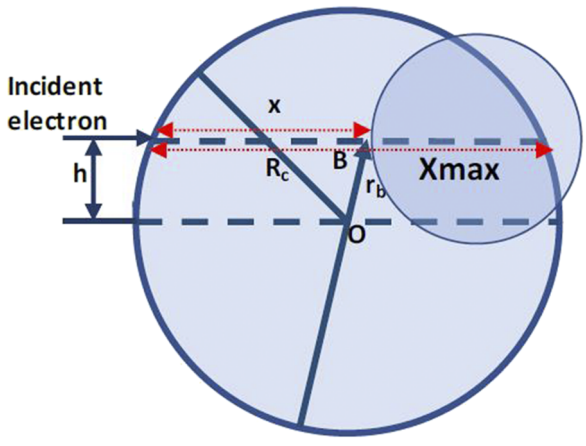

FIG. 2. Spherical model used for modeling the escape probability function $F(x)$.

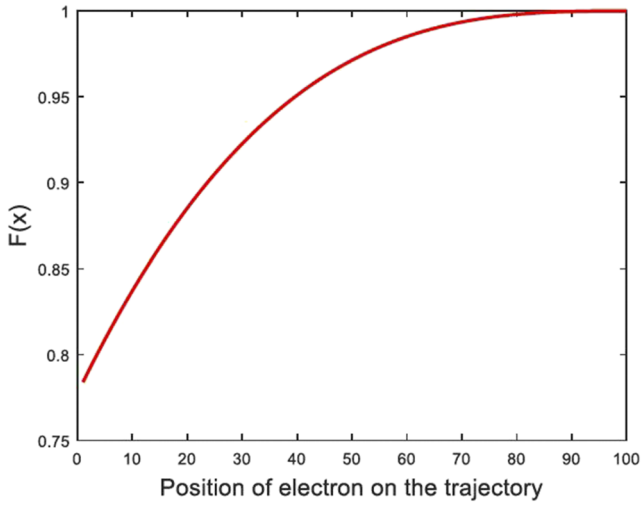

FIG. 3. Escaping probability $F(x)$ with respect to the position of electron on primary electron trajectory.

where the radius of the cluster R_c is a function of cluster size N, as shown in the following equation:

$$R_c = \sqrt[3]{\frac{3NM}{4\pi\rho}}, \tag{8}$$

where M is the molecular mass and ρ is the specific mass of the cluster. Figure 3 shows the probability function $F(x)$ with respect to the position of electron along the trajectory. From the plot, it is observed that when the electron is generated close to the surface of the cluster, the probability is close to 1, which indicates that the electron has a high chance of escaping out of the cluster.

The molecular density n_0 of a cluster is much higher than that of gas. In Ref. 17, the authors approximated the energy loss rate of electrons inside the cluster by formulating an equation, in which the molecular density of cluster was used. For the modeling, we matched the energy loss rates determined by using Eqs. (3) and (4) with the reported empirical energy loss rate of CO_2. Through the process, we derived the molecular density defined by the following equation:

$$n_0 = \frac{4P_c}{kT_c}, \tag{9}$$

where P_c is the critical pressure, T_c is the critical temperature, and k is the Boltzmann constant.

III. RESULTS

With the modeled electron scattering cross section data of various cluster sizes near the critical point, electron kinetic analysis is performed.[19–22] We numerically solve the Boltzmann equation to obtain the density-normalized ionization coefficient (α/N), density-normalized attachment coefficient (η/N), and density-normalized effective ionization coefficient $[(\alpha-\eta)/N]$. The dielectric strength of the clusters of various sizes is represented by the density-normalized critical electric field $[(E/N)_{cr}]$, at which $(\alpha-\eta)/N$ is zero (i.e., the ionization and attachment process are in equilibrium). To validate our study, we model the dielectric strength of supercritical CO_2, which has a critical point of T_{cric} = 304.25 K and p_{cric} = 7.39 MPa. Based on Eq. (1), the electron scattering cross section data of supercritical CO_2 clusters near its critical point are derived from those of gaseous CO_2 retrieved from the Morgan database.[18] Figure 4 shows the attachment, ionization, elastic, and excitation cross sections of supercritical CO_2 with cluster size 25 as a function of electron energy. The cross section data of cluster size 25 are compared with those of gaseous CO_2. According to the figure, it is confirmed that the cross section data of clusters decrease from those of gases. The trend is in agreement with published reports in the literature, in which authors experimentally showed that the electron scattering cross sections of clusters decrease from those of gas species.[25,26] In addition, the authors modeled the breakdown voltage of supercritical CO_2, He, Xe, and H_2O around the critical point based on the electron scattering cross section, ionization potential, and secondary

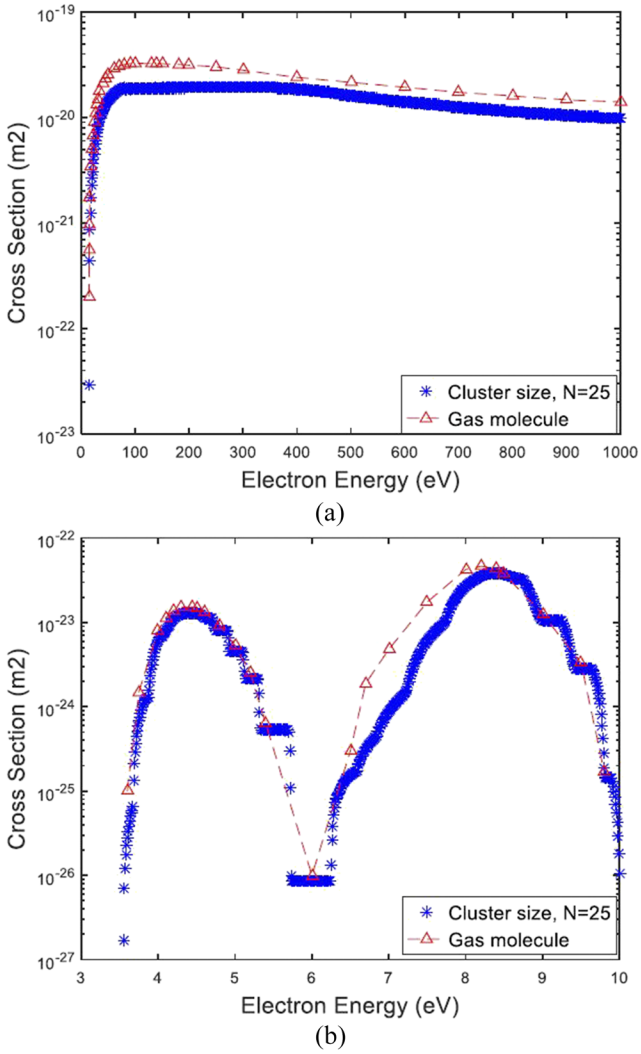

FIG. 4. Electron scattering cross section data of CO_2 with cluster size 25 shown as examples: (a) ionization cross section and (b) attachment cross section.

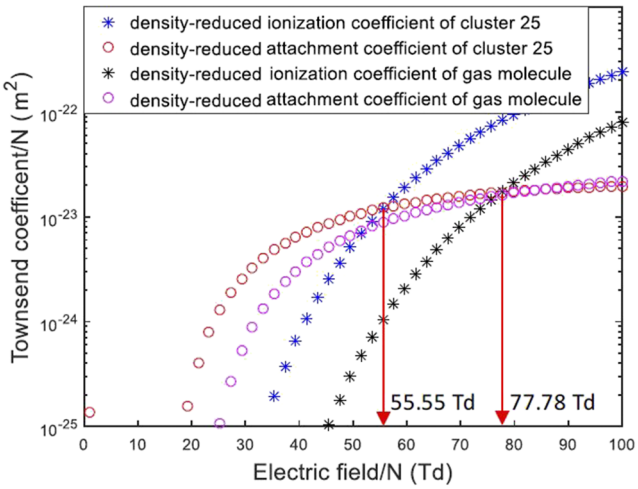

FIG. 5. Density-normalized Townsend coefficients of a CO_2 gas molecule and CO_2 cluster.

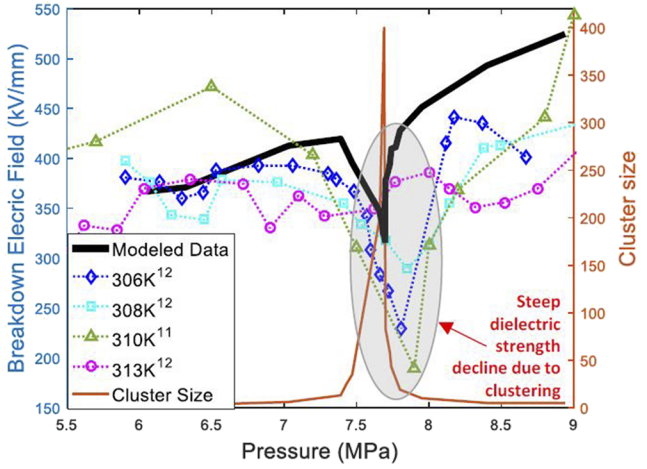

FIG. 6. Dielectric strength of supercritical CO_2 near the critical point. Modeled results agree well with the trends of the experimental data.

Townsend coefficient.[1,11–14] These studies also reported that electron scattering cross section decreases as the cluster size increases around the critical point. α/N and η/N obtained from the Boltzmann analysis are plotted in Fig. 5 as a function of E/N for both gaseous CO_2 and the supercritical CO_2 of cluster size 25. Breakdown strength is represented by $(E/N)_{cr}$. In Fig. 5, it is shown that $(E/N)_{cr}$ of supercritical CO_2 with cluster size 25 decreases to 55.6 Td from the 77.8 Td of gaseous CO_2.

The reduction in $(E/N)_{cr}$ is mainly due to the effect of density fluctuation caused by the formation of clusters near the critical point. Consequently, the dielectric breakdown characteristics of supercritical CO_2 show the steep reduction near the critical point, much lower than the breakdown strength of gas estimated by Paschen's law. Critical electric field E_{cr} derived from various cluster sizes near the critical point are plotted as a function of pressure in Fig. 6. The modeling was conducted assuming a constant temperature of 304.25 K, which is the critical temperature of CO_2. This figure shows that the critical electric field slightly increases with increasing pressure (i.e., Paschen's law), but a sharp decrease occurs as pressure becomes close to the critical point of CO_2 (i.e., cluster formation). We compared the critical electric field values of our model with the experimental values reported in the literature. The experimental values include those corresponding to temperatures from 306 K to 313 K. As shown in Fig. 6, a relatively pronounced dielectric strength decline is observed in the cases of 306 K, 308 K, and 310 K because they are near the critical point. However, almost no decline in dielectric strength is observed in the case of 313 K most likely because the temperature is farther away from the critical point. The modeled dielectric strength of supercritical CO_2 shows the trend of decreasing dielectric strength near the critical point similar to those shown by the experimental data reported in the literature.[11,12]

It is worth noting that the proposed approach of modeling the sharp decline in the breakdown electric field near the critical point is based on the modeled electron scattering cross section data of various sizes of clusters. The approach is different from previously reported modeling methods that rely on the isothermal compressibility data. However, due to the lack of reported experimental data on the cluster sizes of supercritical CO_2 near the critical point, in this study, we assumed the cluster sizes near the critical point, as shown in Fig. 6. Although it was possible to fine-tune the cluster sizes of supercritical CO_2 to achieve closer agreement with the experimental data, we did not do so because the main focus of our study is introducing the new modeling approach. That is, the discrepancies between the modeled data and the reported experimental data can be minimized with accurately measured cluster size data. However, it should be noted that even with more accurate cluster size data, there would always be some level of discrepancies between the data of models and experimental measurements due to the stochastic nature of dielectric breakdown phenomena and finite accuracies in the experimental measurements. In part, this is shown by the uneven experimental data shown in Fig. 6.

IV. CONCLUSIONS

In summary, we modeled the breakdown characteristics of supercritical CO_2 based on the electron scattering cross section data of clusters of various sizes derived from those of gaseous CO_2. A sharp decrease in the critical electrical field occurs near the critical point due to density fluctuation caused by cluster formation. Close agreement was achieved between dielectric strength estimations derived from the electron scattering cross section data of supercritical CO_2 and experimental values reported in the literature. The results support the validity of our modeling approach. In the future, the breakdown characteristics of SCF mixtures of two or more species will be modeled near the critical point based on our electron scattering cross section modeling approach.

DATA AVAILABILITY

The data that support the findings of this study are available within the article.

REFERENCES

[1]S. Stauss, H. Muneoka, K. Urabe, and K. Terashima, "Review of electric discharge microplasmas generated in highly fluctuating fluids: Characteristics and application to nanomaterials synthesis," Phys. Plasmas **22**, 057103 (2015).

[2]Ž. Knez, E. Markočič, M. Leitgeb, M. Primožič, M. K. Hrnčič, and M. Škerget, "Industrial applications of supercritical fluids: A review," Energy **77**, 235 (2014).

[3]Y. Tian, J. Wei, C. Park, Z. Wang, and L. Graber, in *12th International Conference on Properties and Applications of Dielectric Materials (ICPADM)* (IEEE, Xi'an, 2018), pp. 992–995.

[4]J. Wei, C. Park, and L. Graber, "Breakdown characteristics of carbon dioxide-ethane azeotropic mixtures near the critical point," Phys. Fluids **32**, 053305 (2020).

[5]T. Kiyan, T. Ihara, S. Kameda, T. Furusato, M. Hara, and H. Akiyama, "Weibull statistical analysis of pulsed breakdown voltages in high-pressure carbon dioxide including supercritical phase," IEEE Trans. Plasma Sci. **39**, 1729 (2011).

[6]T. Kiyan, K. Tanaka, A. Uemura, M. Takade, B. C. Roy, T. Namihira, M. Sasaki, H. Akiyama, M. Goto, and M. Hara, in *2007 16th IEEE International Pulsed Power Conference* (IEEE, Albuquerque, NM, 2007), pp. 1528–1531.

[7]T. Kiyan, M. Takade, T. Namihira, M. Hara, M. Sasaki, M. Goto, and H. Akiyama, "Polarity effect in DC breakdown voltage characteristics of pressurized carbon dioxide up to supercritical conditions," IEEE Trans. Plasma Sci. **36**, 821 (2008).

[8]T. Kiyan, A. Uemura, B. C. Roy, T. Namihira, M. Hara, M. Sasaki, M. Goto, and H. Akiyama, "Negative DC prebreakdown phenomena and breakdown-voltage characteristics of pressurized carbon dioxide up to supercritical conditions," IEEE Trans. Plasma Sci. **35**, 656 (2007).

[9]T. Furusato, N. Ashizuka, T. Kamagahara, T. Fujishima, T. Yamashita, M. Sasaki, and T. Kiyan, in *2017 IEEE 19th International Conference on Dielectric Liquids (ICDL)* (IEEE, Manchester, 2017), pp. 1–4.

[10]T. Kamagahara, N. Ashizuka, T. Furusato, T. Fujishima, T. Yamashita, M. Sasaki, and T. Kiyan, in *2017 IEEE 19th International Conference on Dielectric Liquids (ICDL)* (IEEE, Manchester, 2017), pp. 1–4.

[11]T. Ito and K. Terashima, "Generation of micrometer-scale discharge in a supercritical fluid environment," Appl. Phys. Lett. **80**, 2854 (2002).

[12]T. Ito, H. Fujiwara, and K. Terashima, "Decrease of breakdown voltages for micrometer-scale gap electrodes for carbon dioxide near the critical point: Temperature and pressure dependences," J. Appl. Phys. **94**, 5411 (2003).

[13]M. Sawada, T. Tomai, T. Ito, H. Fujiwara, and K. Terashima, "Micrometer-scale discharge in high-pressure H_2O and Xe environments including supercritical fluid," J. Appl. Phys. **100**, 123304 (2006).

[14]H. Muneoka, K. Urabe, S. Stauss, and K. Terashima, "Breakdown characteristics of electrical discharges in high-density helium near the critical point," Appl. Phys. Express **6**, 086201 (2013).

[15]H. Muneoka, K. Urabe, S. Stauss, and K. Terashima, "Micrometer-scale electrical breakdown in high-density fluids with large density fluctuations: Numerical model and experimental assessment," Phys. Rev. E **91**, 042316 (2015).

[16]E. Lemmon, M. McLinden, and D. Friend, NIST Standard Reference Database 23: Reference Fluid Thermodynamic and Transport Properties—REFPROP, Version 9.0, National Institute of Standards and Technology, Standard Reference Data Program, Gaithersburg, 2012.

[17]F. Bottiglioni, J. Coutant, and M. Fois, "Ionization cross sections for H_2, N_2, and CO_2 clusters by electron impact," Phys. Rev. A **6**, 1830 (1972).

[18]See http://www.lxcat.laplace.univ-tlse.fr for Morgan database; accessed 30 August 2019.

[19]C. Park, S. Pamidi, and L. Graber, "Boltzmann analysis of cryogenic He-H_2 gas mixtures as dielectric media for high-temperature superconducting power devices," IEEE Trans. Appl. Supercond. **27**, 1 (2017).

[20]C. Park, S. Pamidi, and L. Graber, "The critical electric field of gas mixtures over the extended range of cryogenic operating conditions," J. Appl. Phys. **122**, 153301 (2017).

[21]C. Park, L. Graber, and S. Pamidi, "The dielectric properties of gaseous cryogen mixtures of He, H_2, Ne, and N_2 in a temperature range of 50-80 K at pressures up to 2.0 MPa," J. Appl. Phys. **121**, 083304 (2017).

[22]C. Park, S. Pamidi, and L. Graber, "The dielectric strength of dissociated cryogenic gas media," J. Appl. Phys. **124**, 104104 (2018).

[23]G. J. M. Hagelaar and L. C. Pitchford, "Solving the Boltzmann equation to obtain electron transport coefficients and rate coefficients for fluid models," Plasma Sources Sci. Technol. **14**, 722 (2005).

[24]H. T. Nguyen-Truong, "Modified Bethe formula for low-energy electron stopping power without fitting parameters," Ultramicroscopy **149**, 26 (2015).

[25]W. Henkes and F. Mikosch, "The effective cross section for ionization by electrons of molecules in hydrogen clusters," Int. J. Mass Spectrom. Ion Phys. **13**, 151 (1974).

[26]A. N. Zavilopulo, A. I. Dolgin, and M. A. Khodorkovsky, "Investigation of argon cluster ionization cross sections by electron impact," Phys. Scr. **50**, 696 (1994).